Diffusion/Reaction in Confined Polymer Chains

Cameron F. Abrams,[†] Nam-Kyung Lee,*[,‡,§] and A. Johner[⊥,§]

Department of Chemical and Biological Engineering, Drexel University, Philadelphia, Pennsylvania 19104; Institute of Fundamental Physics, Department of Physics, Sejong University, Seoul 143-743, South Korea; Institut Charles Sadron, 67083 Strasbourg Cedex, France; and Laboratoire Européen Associé ICS (Strasbourg, France)/MPIP (Mainz, Germany)

Received January 9, 2006; Revised Manuscript Received February 24, 2006

ABSTRACT: We discuss theoretically the influence of confinement on diffusion−reaction processes in polymer chains by combining analytical and simulation techniques. This is relevant to intrachain chemical reactions in finely divided media like microemulsions, for temperature-driven collapse of soluble/insoluble copolymers, and for early stages of protein folding where some confinement is achieved by molecular chaperones. It is shown that confinement can accelerate the processes in several ways: (i) by cutting long internal relaxation modes, (ii) by suppressing late stage energy barriers, and (iii) by increasing the initial concentration of reacting sites. Under certain conditions the reaction rates are found to go through a maximum for some intermediate confinement. This is a consequence of the interplay between effects i−iii mentioned above and the screening of hydrodynamic interactions that slows down the reactions.

I. Introduction

Polymeric systems display a variety of interesting irreversible phenomena. In many chemical processes involving polymers, existing chains are driven to react with each other, and specific groups in the polymer sequence can react with foreign oligomeric groups or groups belonging to the same or similar chains. The technological importance of such reactions is considerable. Temperature-driven aggregation of strong specific sticking groups localized along the chain; pairing of amino acids in early stage of protein folding also bear some analogy with it.

Generally speaking, the kinetics of irreversible processes (all the cited processes are at least in some early stages approximately irreversible) is dominated either by diffusion of reactants (usually for fast reactions after contact) or by equilibrium statistics if many contacts are needed on average per effective reaction. In both these situations connectivity in polymer chains plays an important role.[1,2] It was noticed rather early that connectivity entails anomalous diffusion of a given monomer exploring the coil volume.[3] In contrast to free reactants, the short time exploration by a monomer is dense or at least marginally dense in three dimensions. Equilibrium contact statistics is also influenced by connectivity, bringing two monomers of the same or different chains in close vicinity requires on average more contacts between connected monomers. This brings into play the probabilities for formation of higher order vertexes,[4,5] reflected, for example, by des Cloizeaux contact exponents[6] (see Appendix A for more details).

It is often difficult to favor *intrachain* reaction over *interchain* reaction without going to high dilution or to synthesize a very long polymer chain rather than initiating many shorter ones. Recently, it was recognized that finely divided reaction media may offer an elegant way out of these difficulties. When polymerization is conducted in microemulsion rather than in open solution, a single propagation reaction may link (almost) all the monomeric material of one microdropplet into a single very long chain.[7] Similarly, cyclization reactions in microemulsions could be interesting to avoid chain extension reactions. In the same way it should be easy to get single chain aggregates of hydrophobic/polar (H/P) heteropolymers upon collapse if each chain is located in its own microcompartment. More generally, confinement of a polymer chain in any type of box is expected to have a large influence on internal reactions.

We use theoretical arguments to explore the effect of confinement on intramolecular reaction kinetics for generic polymers. There is a trivial concentration effect as the reacting groups are on average closer to each other in the box. Beyond this, when a polymer chain is confined, screening of the hydrodynamic interactions introduces freely draining Rouse dynamics on large scales. The large-scale internal exploration is thus compact rather than marginally compact. The box itself cuts off all internal modes of wavelength larger than the box size. Finally, whenever clusters are to be formed, as in intrachain micellization, high excluded volume barriers are expected in intermediate or late stages. This is expected in H/P copolymer collapse including protein folding. Confinement reduces these excluded volume barriers and eventually suppresses them. In a somewhat similar way molecular chaperones may confine proteins during folding. Recent simulations have set out[8,9] to clarify this point.

In the next section, we will revisit internal cyclization which has previously been investigated by Friedman and O'Shaughnessy.[10,11] We consider two reacting groups separated by a spacer of length s localized in the middle of a long chain in confined media (Figure 1). In section 2.1 we will analytically consider in some details of an ideal chain in a soft box where every monomer is driven toward the origin by a harmonic potential. We will discuss the influence of confinement on the fluctuation of the distance between stickers. These rather detailed studies build a sound basis for semiqualitative arguments in the more relevant case of excluded volume chains. Internal cyclization of excluded volume chain is discussed in section 2.2, and the more general case of many reacting groups is developed in section 3. There, the role of excluded volume barriers in late aggregation is discussed on the basis of standard vertex exponents.[4,6] We also use direct simulation to capture various qualitative aspects of our theoretical picture.

* Corresponding author. E-mail: lee@sejong.ac.kr.
[†] Drexel University.
[‡] Sejong University.
[§] Institut Charles Sadron.
[⊥] Laboratoire Européen Associé ICS/MPIP.

10.1021/ma060044d CCC: $33.50
Published on Web 04/21/2006

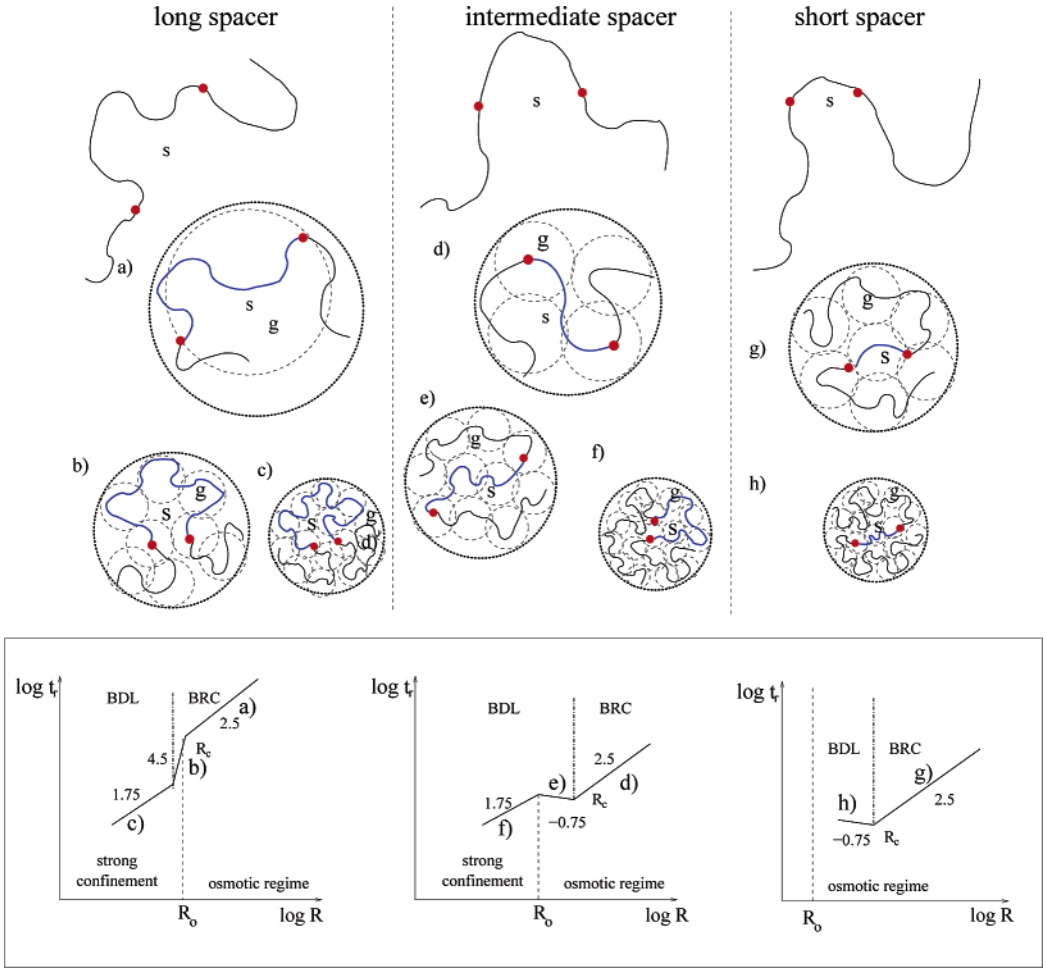

Figure 1. Schematic of a chain with two stickers before and after confinement. Kinetic regimes for long (upper left), intermediate (upper middle), and short (upper right) spacers. Each panel shows regimes of weak (large cavity), intermediate, and strong (small cavity) confinement. The cavity size R dependence of reaction times t_r in various regimes are summarized in the lower panel on a log−log scale. All kinetic regimes (a−e) are identified in the lines with different slopes.

II. Cyclization under Confinement

The special case where a chain only carries two reacting groups separated by a spacer is considered below. The corresponding reaction we call internal cyclization. In contrast to ordinary cyclization involving reacting chain ends, internal cyclization can be seen as the first step toward any higher order *intrachain* association.

Consider two internal labeled groups a distance s apart along a swollen polymer chain (these will later be considered as the sticking groups). Because of ergodicity, long time temporal and spatial conformation sampling are equivalent. After a few relaxation times of the spacer (of length s) t_s, all spacer conformations have been visited according to their statistical weight. Configurations at contact have statistical weight $s^{-3\nu-\nu\theta_2}$ with θ_2 the des Cloizeaux internal contact exponent[6] and ν the Flory swelling exponent (see Appendix A). In the long time limit, the time spent at contact after a total time t is thus $ts^{-3\nu-\nu\theta_2}$. The separation process of the labeled groups after contact is deterministic, driven by excluded volume interactions, as soon as the mutual distance is larger than the monomer size (corresponding to a decrease of energy larger than k_BT). Returns at contact typically only occur after spacer relaxation, and in contrast to the ideal chain case, large correlated return loops after contact are not possible (independently of the chain dynamics). Accordingly, the first passage time for stickers at contact is given by $t_r \sim \tau_0 s^{3\nu+\nu\theta_2}$ with τ_0 a monomeric diffusion time.[12,13] This holds provided $t_r > t_s$. The relaxation of the first passage probability density is exponential for $t > t_s$. The first passage time t_r also gives the reaction time between stickers for fast reaction at contact. We now assume that the relevant relaxation time t_s of the spacer is independent of the total chain length as will be shown later for ideal phantom chains. In Zimm dynamics where hydrodynamic interactions are accounted for $t_s \sim s^{3\nu}\tau_0$, ensuring $t_r > t_s$ as required for consistency. Hence, the reaction time is inversely proportional to the Boltzmann weight of configurations at contact $s^{-3\nu-\nu\theta_2}$. This result is reminiscent of reaction controlled kinetics. The contact exponent θ_2 reflects the excluded volume barrier against sticker contact $W/k_BT \sim s^{\nu\theta_2}$. The result $t_r \sim s^{3\nu+\nu\theta_2}$ is also consistent with those for the Kramers problem where one labeled monomer moves against an external potential, a point of view we will adopt later.

A. Ideal Chain Confined in a Harmonic Box. It is instructive to consider the ideal chain case that accounts for the main effects of connectivity without introducing any other interaction. Furthermore, when the chain is confined in a volume qualitatively smaller than its unperturbed size, excluded volume interactions are essentially screened and the ideal chain model is of some relevance. Similar screening applies to hydrodynamic interactions, and a coarse-grained Rouse model neglecting long-ranged interactions mediated by the solvent is appropriate.

We further specialize to a harmonic box where any monomer is attracted toward the origin by the potential $U = -k_BT(K/2b^2)r^2$, where b is a monomer size. This can be seen as a *soft* box. Minimizing the free energy $F \sim NU(R) + k_BTNb^2/R^2$ of

an ideal chain in the potential fixes the geometrical chain size $R \sim bK^{-1/4}$ in a confining potential ($K > N^{-2}$). This size is independent of the chain length N and can be understood as the size of the soft box. In the free draining limit, the dynamics are governed by the Rouse equation:[14]

$$-\zeta \frac{\partial r_n}{\partial t} + k\frac{k_B T}{b^2}\frac{\partial^2 r_n}{\partial n^2} - K\frac{k_B T}{b^2} r_n + f_n = 0 \qquad (1)$$

The first term stands for the force exerted by the solvent on monomer n at position r_n with ζ the friction, the second for the entropic spring forces exerted on monomer n, and the third for the force exerted by the external harmonic potential with $k = 3$. The last term is the Gaussian random force with zero mean $\langle f_n \rangle = 0$ and delta function correlations, $\langle f_n(t) f_m(t') \rangle = 2\zeta k_B T \delta(m - n)\delta(t - t')$. As the Rouse equation (1) is linear, solutions can be expanded in eigenmodes in terms of Fourier transformed variables X_p, $r_n = 2\sum_{p=1}^{\infty} \exp(-t/\tau_p) X_p \cos(p\pi n/N) + X_0$. The dispersion relation is altered by the harmonic external potential

$$\frac{1}{\tau_p} = k\frac{p^2\pi^2}{N} + K \qquad (2)$$

where we measure time in the unit of monomer self-diffusion time $b^2\zeta/k_B T$. The dynamics are faster as compared to the free chain ($K = 0$). In particular, the center of mass is drifting toward the center of the potential and $\tau_{p=0} = t_K = K^{-1}$ is finite. Generally speaking, this acceleration is most pronounced for the long modes (small p). In particular, the relaxation of modes longer than the box size ($kp^2\pi^2/N \ll K$) is controlled by the box and is close to t_K.

It is worthwhile considering dynamics in the absence of any irreversible reaction. Under the hypothesis of Gaussian noise, any monomer position or relative position obeys Gaussian statistics. Averages and fluctuations thus completely determine the probability distributions of these random variables. The Rouse equation (1) may be solved for the average configuration $\langle r_n(t) \rangle$ corresponding to a given initial configuration $r_n(0)$. It is most instructive to solve for a *central* monomer, thereby neglecting finite size effects. The average position of a given monomer depends on the initial position of all monomers through

$$\langle r_n(t) \rangle = \int_{-\infty}^{+\infty} dn' \, \mathbf{Ker}(|n - n'|, t) r_{n'}(0) \qquad (3)$$

where the kernel $\mathbf{Ker}(x,t) = (1/\sqrt{4\pi kt}) \exp[-x^2/4kt] \exp(-Kt)$ has a finite radius. Qualitatively, the monomer is drifting toward the initial center of mass of the chain segment $(n - n')^2 < 4kt$ where the information has diffused after time t. At larger times $t \geq t_K$ the general drift toward the center of the potential becomes effective. For a given initial configuration, two monomers separated by a contour length s smaller than $1/\sqrt{K}$ thus experience independent drifts at times (much) smaller than the relaxation time of section s.

From eq 1 we obtain fluctuations around the average. As we are merely interested in the internal distances, we will explicitly consider the end-to-end vector distribution of an internal section of contour length s. We take the limit of infinitely long chain where the end effects are negligible. The fluctuation of one component (here the x component of $r_{n+s} - r_n$, $\sigma_s = (x - \langle x \rangle)^2$) reads

$$\sigma_s = b^2\sqrt{\frac{2}{3K}}\left[\mathrm{erf}\sqrt{\frac{t}{t_{box}}}\frac{1}{2}\exp\left(-2\sqrt{\frac{t_s}{t_{box}}}\right)\mathrm{erfc}\left(\sqrt{\frac{t_s}{t_{box}}} - \sqrt{\frac{t}{t_{box}}}\right) + \frac{1}{2}\exp\left(2\sqrt{\frac{t_s}{t_{box}}}\right)\mathrm{erfc}\left(\sqrt{\frac{t_s}{t}} + \sqrt{\frac{t}{t_{box}}}\right)\right] \qquad (4)$$

where $t_s = s^2/4k$ is the characteristic relaxation time of the studied chain section and $t_{box} = 2/K \sim R^4$ is the characteristic time of a section spanning the box. Equation 4 deserves several comments: (1) As expected, the fluctuation around the average does not depend on the initial configuration. (2) In the long time limit, the fluctuation σ_s saturates

$$\sigma_s(\mathrm{eq}) = b^2\sqrt{\frac{2}{3K}}\left(1 - \exp\left(-2\sqrt{\frac{t_s}{t_{box}}}\right)\right) \qquad (5)$$

For a confined chain section the fluctuation saturates at the box size $\sim b^2/\sqrt{K}$, while for an unconfined chain section the fluctuation saturates at the Gaussian fluctuation $\sim b^2 s$. The saturation is slow, $(\sigma_s(\mathrm{eq}) - \sigma_s)/\sigma_s(\mathrm{eq}) \propto \sqrt{t_s/t}$, for an unconfined chain section; it is nonetheless almost completed for a few t_s.[15] (3) In early stages, $t < \min(t_s, t_{box})$, the growth of the fluctuations is governed by anomalous diffusion and

$$\sigma_s = 2b^2\sqrt{\frac{t}{\pi}} \qquad t < \min(t_s, t_{box}) \qquad (6)$$

Next we discuss the reaction time for two monomers located a contour length s apart along a very long chain. If the spacer is not confined, the fluctuation saturates after a few spacer Rouse times t_s. For the ideal chain there is no barrier against contact, and the first passage time at contact is hence of order t_s. The modes longer than s only manifest in the nonexponential relaxation of the fluctuation (at scale t_s). This obviously also holds in the free chain case and justifies the neglect of long modes in the previous subsection.[16] If the reaction is limited by the reaction rate at contact Q, the reaction time is $t_r \sim s^{3/2}\tau_0/Q$ where 3-dimensional Gaussian statistics is assumed. The crossover between the diffusion-limited and reaction controlled regimes hence occurs for $Q\sqrt{s}\tau_0 \sim 1$. For a confined spacer the typical distance between stickers is the box size. The fluctuation of the sticker separation saturates at the box size after the Rouse time of a polymer strand spanning the box, t_{box}. The reaction time is thus $t_r \sim t_{box} \sim (R/b)^4\tau_0$. For slow rate at contact (small Q) $t_r \sim (R/b)^3/Q$, and the crossover is located at $Q\tau_0 R/b \sim 1$.

B. Confined Excluded Volume Chain. In the following, we stick to more general qualitative arguments supported by the internal cyclization in a harmonic box model just discussed in order to take into account excluded volume correlations and hydrodynamics for binding kinetics under confinement. In a recent note, we showed that the interplay between excluded volume correlations and hydrodynamic interactions can produce an optimal confinement where the binding is fastest.[18] In the following we briefly review these results. The interested reader will find more details in ref 18. The blob size separates hydrodynamics and Rouse dynamics. By crowding polymer segments with confinement, a swollen chain turns to a series of blobs. The reaction kinetics is described based on the blob reactions with the coarse-grained blob reaction rate.

We consider a long isolated chain swollen in good solvent with two binding groups a distance s apart in its middle (Figure 1). For binding to take place, the groups must overcome an excluded volume barrier W scaling as $\exp(W/k_B T) \sim s^{\nu\theta_2}$. The

Table 1. Summary of σ_p and Internal Contact Exponents θ Obtained from Ref 5

σ_1	σ_2	σ_3	σ_4	σ_5	σ_6	σ_8	σ_{10}	σ_{12}	σ_{14}	σ_{20}
0.0786	0	−0.2033	−0.4791	−0.8490	−1.2918	−2.377	−2.1355	−3.3522	−4.9302	−10.087
$\nu\theta$	$\nu\theta_{2,2}$	$\nu\theta_{2,4}$	$\nu\theta_{2,6}$	$\nu\theta_{4,4}$	$\nu\theta_{10,10}$	$\nu\theta_{8,12}$	$\nu\theta_{6,14}$	$\nu\theta_{4,16}$	$\nu\theta_{2,18}$	
	0.4791	0.8127	1.085	1.419	5.816	4.3578	3.865	3.22	1.9277	

typical reaction time $t_r \sim s^{3\nu+\nu\theta_2}\tau_0$ for a long spacer can be quite larger than the longest relaxation time of the spacer configuration, $t_s \sim s^{3\nu}\tau_0$, where τ_0 is the diffusion time of a monomer. If the reaction is limited by reaction rate at contact Q,[10] the reaction time is inversely proportional to the probability for reactants to be about one monomer size apart:

$$t_r \sim Q^{-1}s^{3\nu+\nu\theta_2} \tag{7}$$

1. Osmotic Confinement. Some sort of confinement of a labeled chain can be achieved in solution by other identical chains screening excluded volume interactions. There however the labeled chain only shrinks back at most to its Gaussian size. This we term osmotic confinement. It has an interest in its own as the polymers of the bath may be chemically different without necessarily inducing the collpase of the labeled chain in a common good solvent. It is also convenient to discuss it here as a similar regime will appear under moderate geometric confinement.

The solution of spectator chains in good solvents at density c imposes an osmotic pressure $\Pi = k_BTc^{3\nu/3\nu-1}$. This sets a correlation length for density fluctuations associated with the contour length g. By definition, the subsection of size g contributes an internal density of order c; hence $g \sim c^{1/(1-3\nu)}$.

At large enough concentration, the internal section of contour length s ($> g$) turns into an ideal chain of s/g swollen blobs of mass g. The self-diffusion time of a blob is $\tau_b \sim g^{3\nu}\tau_0$ due to the hydrodynamic interactions. The spacers are divided into (s/g) blobs. The typical radius swept by the segment of contour length s is $r_s \sim (s/g)^{1/2}g^{\nu}$. Because hydrodynamic interactions are screened at length scales larger than the blob size, the train of s/g blobs experiences Rouse dynamics (free draining) at scales larger than the blob size. The longest relaxation time of the spacer is $t_s \sim (s/g)^2\tau_b$. Thus, t_s increases due to the screening of hydrohynamic interactions with increasing concentration.

We can qualitatively think of the binding process as internal binding of *blobs* in a chain with a binding rate $Q_b \sim g^{-\nu\theta_2}{\tau_b}^{-1}$ at *blob* contact.[17] The extra factor $g^{\nu\theta_2}$ arises from the excluded volume barrier. For large enough concentration, this no longer depends on spacer size s and is mainly determined by the (much) smaller concentration blob size g (see Appendix).

Depending on the value of Q_b, we may define the two regimes: blob-diffusion limited (BDL) and blob-reaction controlled (BRC). As time goes on after a contact, the spacer spans an increasing volume $g^{3\nu}(t/\tau_b)^{3/4}$. Note that the explored volume grows sublinearly with time; thus, the short time exploration is dense. The average cumulative time in contact after time t increases with time $(t/\tau_b)^{1/4}\tau_b$ for short times ($t < t_s$) and increases linearly for $t > t_s$. Thus, the reaction probability $\mathscr{R}(t)$ at time ($t < t_s$) after the first blob contact is $\mathscr{R}(t) \sim (t/\tau_b)^{1/4}g^{-\nu\theta_2}$, which holds up to $t = t_s$ where

$$\mathscr{P} \sim (s/g)^{1/2}g^{-\nu\theta_2} \tag{8}$$

If Q_b is large ($(s/g)^{1/2}g^{-\nu\theta_2} > 1$), the first blob contact ensures binding. The reaction time is the first passage time of the binding blobs at contact (BDL): $t_r \sim t_s \sim (s/g)^2\tau_b$. Otherwise, the spacer relaxes its configuration at all scales, and several attempts are required for the blob reaction. This results in the BRC reaction time $t_r \sim (s/g)^2\mathscr{P}^{-1}\tau_b \sim (s/g)^{3/2}g^{\nu\theta_2}\tau_b$, reflecting the blob contact probability and Q_b. The reaction time in the osmotic regime is therefore summarized (in units of τ_0):

$$t_r \sim \begin{cases} s^{3/2}g^{3\nu+\nu\theta_2-3/2}, & g > s^{1/(1+2\nu\theta_2)} \quad \text{BRC} \\ s^3g^{3\nu-2}, & g < s^{1/(1+2\nu\theta_2)} \quad \text{BDL} \end{cases} \tag{9}$$

At low osmotic pressure Π, for which $g > s^{1/(1+2\nu\theta_2)}$, the reaction time decreases upon increasing the density as $t_r \propto g^{3\nu+\nu\theta_2-3/2}$. However, at high osmotic pressure, the reaction time increases upon increasing the density as $t_r \propto g^{3\nu-2}$. This means that the binding rate goes through a maximum at the cross over from BRC to BDL. The binding kinetics are fastest at optimum blob size:

$$g_{opt} \sim s^{1/(1+2\nu\theta_2)} \tag{10}$$

The exponents $\nu\theta_2$ may be approximated as $\nu\theta_2 = 0.479$ (see Table 1); thus, the s exponent for optimum is close to 1/2.

2. Geometrical Confinement. More explicit confinement can be achieved by a geomtric constraint (e.g., Figure 1a−e). If a chain of total length N is confined within a sphere of radius $R < N^{\nu}$, the local scale g is fixed by the imposed monomer density

$$N/R^3 \sim g^{1-3\nu} \tag{11}$$

and decreases upon confinement. This sets the "critical" cavity size

$$R_0 \sim s^{1/2}g^{\nu-1/2} \sim s^{3\nu-1}N^{1-2\nu} \tag{12}$$

for strong confinement below which the spacer is reflected by the boundary.

At moderate confinement (Figure 1a,d) where the cavity size is still larger than the critical size for the spacer confinement ($R_0 < R < N^{\nu}$) the osmotic regime described previously applies. There is an optimum confinement at crossover from BRC to BDL when the blob size is g_{opt} (eq 10), which corresponds to the cavity size:

$$R_c \sim N^{1/3}s^{(3\nu-1)/3(1+2\nu\theta_2)} \tag{13}$$

To find an optimum, the condition $R_c > R_0$ should hold. The spacer length s should be short enough to satisfy the condition: $N > s^{3/2[-1/(2(1+2\nu\theta_2))]}$. The reaction time t_r eq 9 can be written in terms of the confinement cavity size using eq 11. In BRC and BDL regime $t_r \sim R^{2.5}$ and $t_r \sim R^{-0.75}$, respectively. The negative kinetic exponent in BDL regime (−0.75) indicates the reaction is slower as the confinement cavity size is smaller.

In the strong confinement regime ($R < R_0$) (Figure 1b,c), the spacer is so long that it is reflected by the confining boundary. For too short spacer all solvent can be (formally) expelled before reaching the strong confinement regime for the spacer. This imposes the physical constraint $N < s^{3/2}$ for the existence of the strong confinement regime for the spacer. The longest relaxation time is set by the box size R as $(R/g^{\nu})^4\tau_b$. Long spacers ($N < s^{3/2[-1/(2(1+2\nu\theta_2))]}$) experience the strongly confined BRC regime, and the reaction time is $t_r \sim (R/g^{\nu})^3g^{\nu\theta_2}\tau_b$. The blob size can be still large (low Q_b) even though the spacer is reflected by the wall. The crossover to BDL occurs at

$$R_c^{(s)} \sim N^{(\nu+\nu\theta_2)/(1+3\nu\theta_2)} \tag{14}$$

and it is smaller than R_0. For smaller cavity size, BDL regime applies and no optimum appears in strong confinement. The binding rate become faster in both BRC and BDL regime with increasing confinement.

$$t_r \sim \begin{cases} R^{3(1+\nu\theta_2/(3\nu-1))} N^{-\nu\theta_2/(3\nu-1)} \sim R^{4.5}, & R > R_c^{(s)} \text{ BRC} \\ R^{4-[3\nu/(3\nu-1)]} N^{\nu/(3\nu-1)} \sim R^{1.75}, & R > R_c^{(s)} \text{ BDL} \end{cases} \tag{15}$$

We summarize the kinetic regimes in the lower panel of Figure 1. The reaction time t_r vs the cavity size R in log−log scale ($t_r \propto R^{\beta}$) after eqs 11 and 9 (osmotic regime) and eq 15 (strong confinement regime). The exponent β (indicated as the slope) is approximately 4.5, 1.75, −0.75, 2.5 for BDL and BRC in strong confinement and BDL and BRC in osmotic regimes, respectively. R_o separates osmotic and strong confinement regimes, and R_c separates blob reaction controlled (BRC) and blob diffusion limited (BDL) regimes.

Langevin dynamics simulations of single bead−spring chains separately (a) under the influence of a harmonic confining potential and (b) geometrically confinged in spherical cavities were performed to verify qualitative aspects of the reaction kinetics. Simulation details are presented in Appendix B. For various strengths of the confining potential, K (eq 1), as well as for various sizes of cavities R, we measure the internal cyclization time, t_r, for chains of length $N = 102$ with stickers at positions 26 and 77 ($s = 50$). We consider both ideal (phantom) chains (no excluded volume interactions apart from nearest neighbors along the contour) and excluded volume chains. As these are Langevin dynamics simulations, Rouse dynamics is expected to hold. In Figure 2a, we show t_r vs K for ideal chains. We observe $t_r \sim R^4$ ($\sim K^{-1}$) over an intermediate domain of K, as expected.

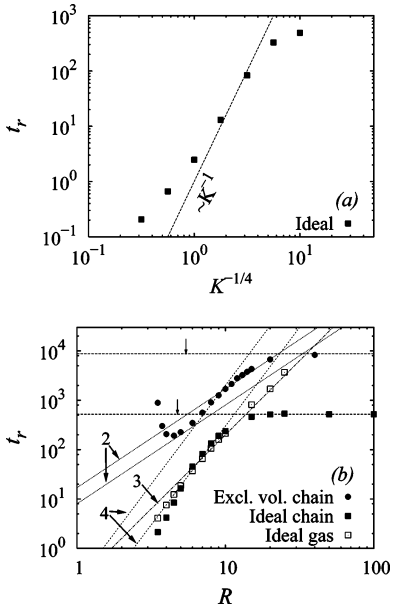

Figure 2. Results from Langevin dynamics simulations for chains of length $N = 102$ with two stickers separated by a spacer of length $s = 50$ in the middle of the chain. (a) Reaction time vs confining potential strength (eq 1) for an ideal chain. (b) Reaction time vs cavity radius for geometrically confined excluded volume and ideal chains. Horizontal line denotes saturation of t_r, and arrows indicate the respective unperturbed radii of gyration. Numbers labeling each line denote scalings with R. In both (a) and (b), each point is an average of 1000 independent trajectories.

In Figure 2b, we show t_r vs R for both ideal and excluded volume chains as well as for an equivalent "ideal gas" of two sticker particles with no bonds (but with a finite cutoff for the sticker−sticker attractive interaction). For the ideal gas, we see that $t_r \sim R^3$ as expected for a trivial dependence on concentration. For the ideal chain t_r saturates above $R = 10$ where confinement becomes irrelevant due to connectivity. Below $R = 7$, the spacer is reflected by box boundary, and the reaction time t_r scales with R as $t_r \sim t_{box} \sim R$.[4] As predicted in section 2.1, connectivity makes the curve steeper. At smaller cavity size, the increased sensitivity is due to the long-range sticker−sticker interaction: stickers attract each other at a distance of 4 (the pair potential cutoff; see Appendix B). When the average distance between stickers is comparable to the range of attraction, the reaction becomes potential driven and thus deterministic. This increases the sensitivity on R for the ideal gas; these data establish that the ideal chain is more sensitive to R than the ideal gas, which we attribute to connectivity rather than to the attractive interaction alone. For the excluded volume chains, we observe a mininum t_r at about $R = 4$, below which t_r increases severely with decreasing R due to increased restriction of monomer mobility (monomers are effectively frozen at this concentration.) Above $R = 4$, t_r shows transitions from a regime in which $t_r \sim R^2$ to $t_r \sim R^4$ and again to $t_r \sim R^2$. The steep changes at intermediate cavity size qualitatively agree with the theory for long spacers.

Because hydrodynamics are not explicitly included, the simulations do not reflect the most important aspect of the theoretical predictions, namely the maximum reaction rate between BRC and BDC regimes. Ongoing simulations are underway to investigate this aspect, but they are enormously expensive due to the need to include explicit solvent particles.

III. Multiple Binding

A. Formation of Higher Order Vertices. Internal cyclization, presented above, corresponds to the fusion of two 2-leg vertices into a 4-leg vertex. In internal micellization, for example, sticking groups assemble in clusters with higher order aggregation numbers corresponding formally to higher order vertices[19] (Figure 3a). A p-leg vertex is governed by the vertex exponent σ_p. For example, the contact exponent θ_2 obeys $\nu\theta_2 = -\sigma_4$. Up to very recently, little was known regarding the values of the vertex exponents besides ϵ-expansions that only correctly describe low-order vertices. In a very recent simulation, Grassberger[5] measured partition functions Z_p of polymer stars up to 80 arms. These results allow one to extract σ_p through $Z_p \sim N^{\gamma_p - 1}$ with $\gamma_p - 1 = \sigma_p + p\sigma_1$. The obtained values of σ_p are displayed in Table 1 for p ranging from 1 to 20. There is fair agreement between the simulation and values of the exponents obtained after resummation of the ϵ-expansion by von Ferber.[20]

For large number of arms p, the Daoud−Cotton limit[21] should apply, which predicts $\gamma_p - 1 \propto -p^{3/2}$. Taking numerical estimates from Grassberger,[5] the best fit to the higher order vertices (up to 60 where the legs are still fairly large) gives the prefactor 0.2: $\gamma_p - 1 = \sigma_p + p\sigma_1 \approx -0.2p^{3/2}$.

The Daoud and Cotton model is simple enough to allow for a detailed study of a polymer star immersed in a semidilute solution with a concentration blob size g (see Figure 3b). The corona has locally the structure of a semidilute solution where the blob size $g(r)$ corresponds to the local blob size. Chains in the corona are stretched at scales larger than the blob radius $\xi(r)$. Each blob is spanned by one leg (at the scaling level). Assuming that a finite fraction of the legs starts beyond the distance r, the blob size ξ grows with the distance to the center

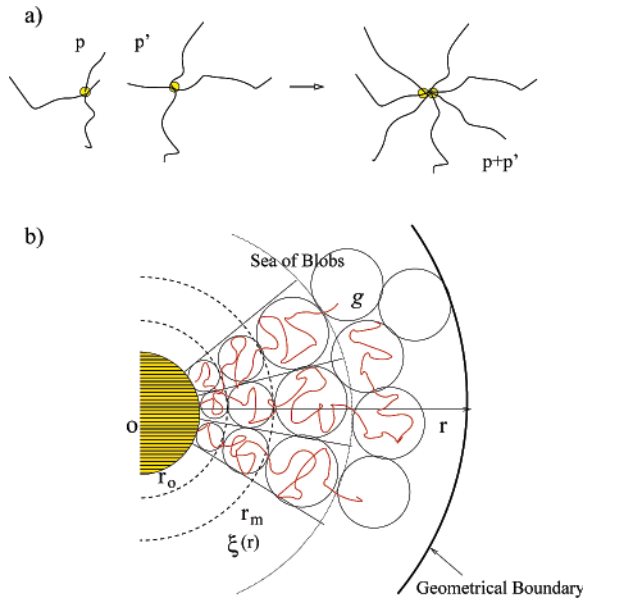

Figure 3. (a) Illustration of high order vertex formation. (b) A *p*-arm micelle under confinement. For large number of arms, the Daoud−Cotton limit applies. r_0 and r_m stand for the size of hydrophobic core and the radius, respectively. The blob size saturates at $\rho > r_m$ due to the imposed boundary.

as $r/\sqrt{p}$ and saturates at $\xi \sim g^{\nu}$ in the sea of blobs. In the sea of blobs, the blob size is roughly constant and set to g by the osmotic pressure. This happens for a distance from the center $r > bg^{\nu}\sqrt{p}$. Beyond this distance the arms are still stretched, and we may consider the star as a molten star of blobs up to a distance $bg^{\nu}p$ (for long enough chains) beyond which the accumulated stretching energy per leg is less than the thermal energy. The stretching energy of this region where foreign monomers do not penetrate is dominated by the lower boundary and amounts to $\sqrt{p}$ per leg. The free energy of the star remains hence dominated by the internal corona where the blob size is not uniform:

$$F/p = \int_{r_o}^{r_m} \frac{dr}{\xi} = p^{1/2} \int_{r_o}^{r_m} \frac{dr}{r} = p^{1/2} \ln\left(1 + \frac{r_m}{r_o}\right) \qquad (16)$$

where r_o is size of the hydrophobic core and r_m is the position of the largest blob which is set up by concentration due to the confinement. If $r_m \gg r_o$, then $r_m/r_o \approx g^{\nu}\sqrt{p}$, and eq 16 takes the standard form if the (weak) vertex dependence corresponding to arm stretching is dropped under the logarithm. The blob size saturates at a smaller radius as the confinement cavity size decreases. The total free energy of the *p*-arm star is $\sim p^{3/2}$ log-$(g^{\nu}\sqrt{p})$. Nonetheless, the outer layer of the molten blob legs determines long-ranged interactions and may not be negligible for short legs. It merely multiplies the argument of the log by a constant of order unity. The excluded volume barrier for higher order vertice fusions $p + p'$ is thus expected to grow with vertex order as $0.2((p + p')^{3/2} \log(g^{\nu}\sqrt{p+p'}) - p^{3/2} \log(g^{\nu}\sqrt{p}) - p'^{3/2} \log(g^{\nu}\sqrt{p'}))$.

For vertices of order less than about 20, the Daoud and Cotton model cannot be expected to be accurate.[5] Instead, we may proceed as we did for internal cyclization. The fusion of two higher order vertices of order p and p' follows rules similar to internal cyclization, with the corresponding contact exponent $\theta_{p,p'}$ given by $\nu\theta_{p,p'} = -\sigma_{p+p'} + \sigma_p + \sigma_{p'}$.

As can also be seen from Table 1, the barriers ($s^{\nu\theta}$) against fusion of higher order vertices in dilute solution can be quite high even for moderate spacers. We thus expect intermediate aggregates to be metastable. Under osmotic confinement the barriers can be drastically reduced as they go with a high power of concentration for high vertices. The discussion of BRC vs BDL parallels that for internal cyclization. At low densities, kinetics of the fusion is in BRC regime and the binding rate Q_b reflects the energy barrier for cluster formation with higher order vertices: $Q_b \sim g^{-\nu\theta_{p,p'}}\tau_b^{-1}$. The optimum shifts to higher densities for higher order vertices and can be obtained from eq 10 by replacing θ_2 by $\theta_{p,p'}$. The optimum can be reached for a number of fusion with reasonable spacer sizes. As an example, for fusion of a doublet ($p = 2$) and an isolated sticker ($p' = 1$), $\nu\theta_{2,1} = 0.813$ and $g_{opt} \sim s^{0.381}$, whereas for two doublets $\nu\theta_{2,2} = 1.419$ and $g_{opt} \sim s^{0.260}$. This formulation applies to vertices of any order but does not directly allow one to discuss corrections as the effect of the outer corona belonging to the sea of blobs. At high densities, a number of fusions are governed by blob diffusion and are thus independent of the vertex exponents. The corresponding binding rates are essentially the same in BDL regime. Confinement may thus partially destroy the hierarchy of fusions that prevails for free chains with large spacers s. As for internal cyclization the spacer size plays no role under strong confinement where the spacer is reflected by the boundary, and no optimum confinement is expected.

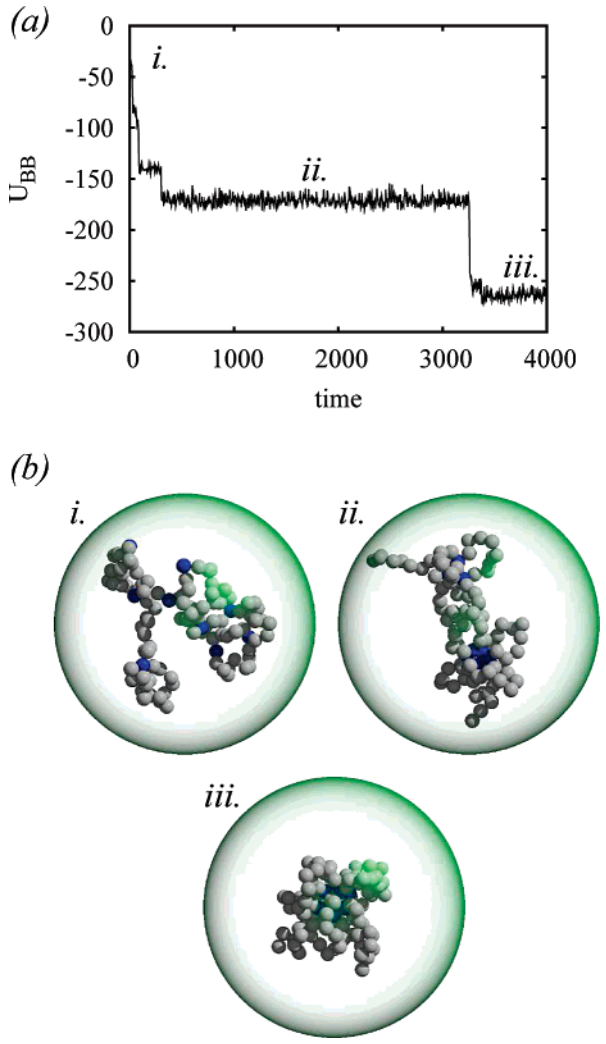

Figure 4. Langevin dynamics simulation results for internal micellization of a 10-sticker heteropolymer: One representative trajectory from the $R = 9$ data set. (a) Trace of sticker−sticker attractive potential U_{BB}. (b) Snapshots of the (i) open coil, (ii) two-core metastable intermediate, and (iii) the final stable single-core micelle.

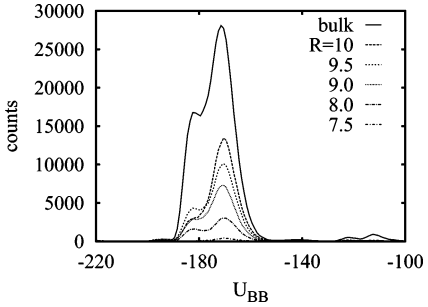

Figure 5. Lifetime distributions of two-core metastable states for various confining cavity radii from Langevin dynamics simulations of 10-sticker chains.

Simulations also confirm the presence of barriers to the formation of higher order vertices (again, details appear in Appendix B). An example collapse trajectory of a 10-sticker heteropolymer is depicted in Figure 4, for which the size of the cavity is $R = 9$. Figure 4a shows a trace of the attractive B−B potential energy over a 4000τ trajectory. The appearance of metastable intermediates is obvious from this plot. Snapshots (Figure 4b) reveal the nature of the metastable intermediates: the two-core intermediate is stable for many thousands of τ in this particular trajectory. The two-core metastable intermediate is separated from the single-core stable ground state by an energy barrier related to the higher order vertex exponent introduced above.

We can obtain a qualitative understanding of the effect of confinement on this barrier by asking how confinement alters the lifetime of this metastable state. For each R, we performed a histogram analysis of the observed B−B potential energy. Because each run was terminated at an arbitrary time after first detecting the single-core state, the histograms represent raw counts of how often a B−B energy in each bin was observed. We show these raw histograms in Figure 5. From these data, we can see that confinement significantly alters the metastable lifetimes in the BRC regime: the smaller the confining cavity's radius, the larger the polymer concentration. Thus, the energy barrier separating the two-core intermediate from the single-core configuration is reduced, akin to the prediction of eq 16. Further confinement brings the system into the BDL regime where the energy barrier is irrelevant.

IV. Conclusions

Internal cyclization was shown to depend on confinement in a rather complicated way depending on the quality of solvent and the degree of confinement. In the simulation, Rouse dynamics and excluded volume statistics are implemented which leads to a monotonic decrease of the cyclization time upon confinement. An intermediate regime is detected where the variation of the reaction time is steepest, in agreement with theory.

When hydrodynamic interactions are accounted for theoretically, a much richer behavior of the reaction time is predicted. Several effects are competing upon confinement. At weak confinement reduction of excluded volume fastens the reaction (BRC). At somewhat stronger confinement (BDL, no spacer reflection) screening of hydrodynamic interactions slows down the kinetics. At strong confinement (spacer reflection), relaxation times of long spacer modes saturate at t_{box} (the relaxation time of a strand spanning the box with Rouse/Zimm dynamics), and the kinetics is accelerated again. For short spacers the reaction time goes through a minimum at some optimal confinement where the binding is fastest. The optimum is located at the crossover from the blob reaction controlled to the blob diffusion limited regimes at moderate confinement where the spacer is not yet squeezed. For somewhat longer spacers, the minimum turns into a local minimum, while a new local maximum appears at the onset of spacer confinement. The binding is fastest at maximum compression. For long spacers the crossover from the blob reaction controlled to the blob diffusion limited regimes falls in the strong confinement regime where the spacer is squeezed and the reaction time monotically decreases upon confinement. When hydrodynamics are accounted for in the tricritical regime (close to the θ-point), binding kinetics is always blob diffusion limited, and only the local maximum remains.

Similar results were obtained in the case of the formation of higher order aggregates. The optimal confinement shifts to higher densities for larger aggregates. For spacer length s between aggregates $g_{opt} \sim s^{0.381}$ for fusion of a doublet and a singulet, whereas for two doublets $g_{opt} \sim s^{0.260}$ and for a quadruplet and sextuplet $g_{opt} \sim s^{0.103}$, which corresponds to a high polymer volume fraction for reasonable spacer length. Beyond optimal confinement, and more generally in the Blob diffusion limited regime, the reaction no longer depends on the vertex degree. At a given confinement several low-order vertices may form at very similar rates. In contrast, at low or no confinement when barriers against fusion are relevant some intermediate size metastable clusters are predicted and also found in simulations (run with Rouse dynamics).

For our scaling analysis to apply, length scales should be fairly separated. The radius of the spacer should hence be markedly smaller than that of the whole chain. The optimal blob size should be swollen. In the weak coupling limit for excluded volume this requires a minimal blob size (10 monomers is typical); in the strong coupling limit (relevant for most simulations) small blobs are actually slightly overswollen and there is no true lower blob size limit.

Acknowledgment. N.-K. Lee acknowledges financial support from Université Louis Pasteur, Strasbourg (Professeur invité), and from the KOSEF/CNRS exchange program. C. F. Abrams acknowledges the donors of the American Chemical Society Petroleum Research Fund for partial support of this research.

Appendix A. Contact Exponents

Contact exponents were introduced by des Cloizeaux for the contact probability between points of a single chain.[4,6] The contact probability that two extremities of a segment inside a single chain are at a relative distance x is

$$P_a(x) \sim (R)^{-d} F_a(x/R) \qquad \text{(A1)}$$

where the scale R is the swollen size of the segment. $F(z)$ is a universal function which depends on the location of the considered segment along the chain.

$$F_a(z) \sim z^{\theta_a} \; (z \to 0) \qquad a = 0, 1, 2 \qquad \text{(A2)}$$

The des Cloizeaux contact exponent θ_a distinguishes three different pair types shown in Figure 6. By convention, $a = 0$ corresponds to the two extremities of a chain $a = 1$ to the contact of one extremity inside the chain and $a = 2$ to that of the internal points. The larger exponent for the internal points is due to the excluded volume effect.

Appendix B. Simulation Description

To characterize some aspects of the kinetics under confinement, Langevin dynamics simulations were performed on linear

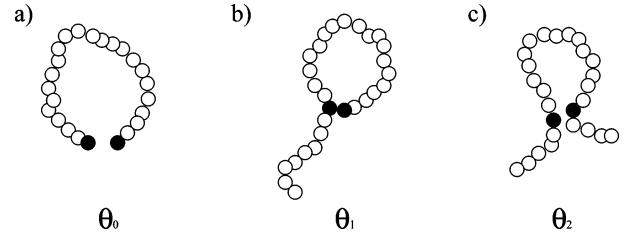

Figure 6. des Cloizeaux's contact exponent: θ_0, θ_1, and θ_2 correspond respectively to the contact of two extremities of a chain ($a = 0$), to the contact of one extremity inside the chain ($a = 1$), and to that of the internal points ($a = 2$) ($\theta_2 > \theta_1 > \theta_0$). Configurations at contact have statistical weight reduced by the factor $s^{\nu\theta_i}$ ($i = 0, 1, 2$) which reflects the excluded volume barrier.

heteropolymers in rigid spherical cavities. Two situations are considered: internal binding in chains with two stickers and internal aggregation chains with 10 stickers. In the first case, we consider polymer chains of length $N = 102$ with two stickers (B-monomers) separated by spacer length 50. The sequence structure of such a chain is expressed as $A_{25}BA_{50}BA_{25}$, where "B"-type monomers are attracted to each other under reaction conditions. The second setup aims for the kinetics of higher order vertices, and here we consider heteropolymers with the sequence $(A_9B)_{10}A_9$.

Reaction conditions are defined such that, upon contact, the B-type monomers aggregate irreversibly, while members of nonbonded A−A and A−B pairs repel one another equally. Repulsive interactions are modeled using the Weeks−Chandler−Andersen potential:[22]

$$U_{\mathrm{WCA}}(r) = \begin{cases} 4\epsilon\left[\left(\frac{\sigma}{r}\right)^{12} - \left(\frac{\sigma}{r}\right)^{6} + \frac{1}{4}\right] & r < 2^{1/6}\sigma \\ 0 & r > 2^{1/6}\sigma \end{cases} \quad \text{(B1)}$$

B−B attractive interactions are modeled using the standard Lennard-Jones potential, $U_{\mathrm{LJ}}(r)$, with a well depth ϵ of 10.0 and cutoff at $r = r_c = 4.0\sigma$. A shift is added to U_{LJ} such that $U_{\mathrm{LJ}}(r_c) = 0$:

$$U_{\mathrm{LJ}}(r) = \begin{cases} 4\epsilon\left[\left(\frac{\sigma}{r}\right)^{12} - \left(\frac{\sigma}{r}\right)^{6} + \left(\frac{\sigma}{r_c}\right)^{12} + \left(\frac{\sigma}{r_c}\right)^{6}\right] & r > r_c \\ 0 & r > r_c \end{cases} \quad \text{(B2)}$$

A standard Lennard-Jones reduced unit system is adopted in which the particle mass is unity ($m = 1$) and length is measured in units of particle diameter, σ, and energy in units of ϵ. Time is measured in units of $\tau = \sigma\sqrt{m/\epsilon}$. This simple prescription is similar to that used to drive phase separation in homopolymer collapse simulations,[23−25] and in simulations of polysoap intramolecular micellization.[19] Particles are connected to each other along the backbone of a chain using via the FENE/WCA potential with the standard values $a = 30.0\epsilon$ and $R_0 = 1.5\sigma$:[26]

$$U_{\mathrm{FENE/WCA}}(r) = U_{\mathrm{WCA}}(r) + U_{\mathrm{FENE}}(r)$$

$$U_{\mathrm{FENE}}(r) = -\frac{a}{2}R_0^{\,2}\ln\left[1 - \left(\frac{r}{R_0}\right)\right] \quad \text{(B3)}$$

Simulations are conducted in the canonical ensemble by using modified particle equations with Langevin-type random and dissipative forces:[26]

$$\ddot{\mathbf{r}} = \mathbf{F} - \Gamma\dot{\mathbf{r}} + \mathbf{W} \quad \text{(B4)}$$

where the friction coefficient, Γ, and the random force, $\mathbf{W}$, together satisfy a fluctuation−dissipation relation:

$$\langle \mathbf{W}_i(t)\cdot\mathbf{W}_j(t')\rangle = 6\delta_{ij}\delta(-t')k_{\mathrm{B}}T\Gamma \quad \text{(B5)}$$

The particle equations of motion are integrated using the velocity-Verlet algorithm,[27] with a time step Δt of 0.01τ and with a friction $\Gamma = 1.0$.

We consider confinement via either a harmonic confining potential as introduced in eq 1, represented by the constant K, or by a geometrically confining spherical cavity of radius R. For harmonic confinement, each monomer is subject to the one-body potential:

$$U_{\mathrm{H}}(r) = \frac{Kr^2}{2} \quad \text{(B6)}$$

where r is the distance from the origin. In the case of geometrical confinement, the confining sphere walls interact with each monomer through a repuslive 10−4 potential:

$$U_{10-4}(r) = \begin{cases} 2\pi\epsilon_w\sigma_w^{\,2}\left[\frac{2}{5}\left(\frac{\sigma_w}{r}\right)^{10} - \left(\frac{\sigma_w}{r}\right)^{4} + \frac{3}{5}\right] & r < \sigma_w \\ 0 & r \geq \sigma_w \end{cases} \quad \text{(B7)}$$

where r is distance from the particle to the wall:

$$r \equiv R - |\mathbf{r}_i| \quad \text{(B8)}$$

For each value of either K or R, 1000 independently realized initial conditions are simulated, beginning from a relaxed open coil. The procedure for a single collapse trajectory is as follows. A run is initialized by first growing a single chain in a box as a nonreversal random walk with a step length $l = 0.97$. In the case of geometrical confinement, the walk is confined within the cavity (i.e., no monomer is allowed to venture a distance more than R from the origin). Any particle overlaps are removed by performing a few thousand integration time steps with a pairwise force cap that increases incrementally each time step until it is no longer triggered. The chains are further relaxed for 5000 more integration steps. At this instant, the quench into selective solvent conditions is performed via instantaneously "switching on" attraction in B−B pairs. This NVT MD integration is typically run until a predefined stopping condition is met. For the two-sticker chains, we choose this condition to be when the distance between the two B-type monomers is less than 1.5. For 10-sticker chains, we terminate when all stickers belong to one micellar core. All simulations were run on AMD Athlon MP2200+ processors. All runs were performed at $T = 1.0$.

References and Notes

(1) Wilemsky, G.; Fixman, M. *J. Chem. Phys.* **1974**, *60*, 866.
(2) Doi, M. *Chem. Phys.* **1975**, *9*, 455.
(3) de Gennes, P. G. *J. Chem. Phys.* **1992**, *76*, 3316.
(4) Duplantier, B. *J. Stat. Phys.* **1989**, *54*, 581.
(5) Hsu, H.-P.; Nadler, W.; Grassberger, P. *Macromolecules* **2004**, *37*, 4658.
(6) des Cloizeaux, J. *Phys. Rev. A* **1974**, *10*, 1665.
(7) Chow, P. Y.; Gan, L. M. *Adv. Polym. Sci.* **2005**, *175*, 257−298.
(8) Klimov, D. K.; Newfield, D.; Thirumalai, D. *Proc. Natl. Acad. Sci. U.S.A.* **2002**, *99*, 8019.
(9) Sliozberg, Y.; Abrams, C. F. *Macromolecules* **2005**, *38* 5321.
(10) Friedman, B.; O'Shaughnessy, B. *Macromolecules* **1993**, *26*, 4888; *Phys. Rev. A* **1989**, *40*, 5950.
(11) Friedman, B.; O'Shaughnessy, B. *Europhys. Lett.* **1993**, *21*, 779.
(12) Rubinstein, M.; Semenov, A. N. *Macromolecules* **1998**, *31*, 1386.
(13) Baljon, A. R. C. *Macromolecules* **1993**, *26*, 4339.
(14) Doi, M.; Edwards, S. F. *The Theory of Polymer Dynamics*; Clarendon Press: Oxford, 1989.
(15) Here the larger t_{box} is formally infinite.
(16) For the finite free chain the terminal relaxation is exponential and determined by the longest Rouse time of the chain; this however sets in close to saturation for a deviation as small as s/N.

CDV

(17) If monomer/monomer binding is limited by the reaction rate at contact Q, Q_b is multiplied by $Q\tau_0$.
(18) Lee, N.-K.; Abrams, C. F.; Johner, A. *Europhys. Lett.* **2005**, *72*, 922.
(19) Lee, N.-K.; Abrams, C. F. *J. Chem. Phys.* **2004**, *121*, 7484.
(20) von Ferber, Ch.; Holovatch, Yu. *Condens. Matter Phys.* **2002**, *5*, 117.
(21) Daoud, M.; Cotton, J. P. *J. Phys. (Paris)* **1982**, *43*, 531.
(22) Weeks, J. D.; Chandler, D.; Andersen, H. C. *J. Chem. Phys.* **1971**, *54*, 5237.
(23) Chang, R.; Yethiraj, A. *J. Chem. Phys.* **2001**, *114*, 7688.
(24) Abrams, C. F.; Lee, N.-K.; Obukhov, S. *Europhys. Lett.* **2002**, *59*, 391.
(25) Polson, J. M.; Zuckermann, M. J. *J. Chem. Phys.* **2002**, *116*, 7244.
(26) Kremer, K.; Grest, G. S. *J. Chem. Phys.* **1990**, *92*, 5057.
(27) Swope, W. C.; Anderson, H. C.; Berens, P. H.; Wilson, K. R. *J. Chem. Phys.* **1982**, *102*, 2851.
(28) Abrams, C. F.; Kremer, K. *J. Chem. Phys.* **2001**, *115*, 2776.

MA060044D